Effects of extracellular calcium on cell membrane resealing in sonoporation

Yun Zhou [a], Jingyi Shi [b], Jianmin Cui [b], Cheri X. Deng [a,c,*]

[a] *Department of Biomedical Engineering, Case Western Reserve University, Cleveland, OH, USA*
[b] *Department of Biomedical Engineering, Washington University, St. Louis, MO, USA*
[c] *Department of Biomedical Engineering, University of Michigan, 2200 Bonisteel Boulevard, Ann Arbor, MI 48109-2099, USA*

Abstract

Sonoporation has been exploited as a promising strategy for intracellular drug and gene delivery. The technique uses ultrasound to generate pores on the cell membrane to allow entry of extracellular agents into the cell. Resealing of these non-specific pores is a key factor determining both the uptake and post-ultrasound cell survival. This study examined the effects of extracellular Ca^{2+} on membrane resealing in sonoporation, using *Xenopus* oocytes as a model system. The cells were exposed to tone burst ultrasound (1.06 MHz, duration 0.2 s, acoustic pressure 0.3 MPa) in the presence of 0.1% Definity® at various extracellular $[Ca^{2+}]$ (0–3 mM). Sonoporation inception and resealing in a single cell were monitored in real time via the transmembrane current of the cell under voltage clamp. The time-resolved measurements of transmembrane current revealed the involvement of two or more Ca^{2+} related processes with different rate constants and characteristics. Rapid resealing occurred immediately after ultrasound application followed by a much slower resealing process. Complete resealing required $[Ca^{2+}]$ above 0.54 mM. The cells resealed in 6–26 s at 1.8 mM Ca^{2+}, but took longer at lower concentrations, up to 58–170 s at 0.54 mM Ca^{2+}.
© 2007 Elsevier B.V. All rights reserved.

Keywords: Sonoporation; Ultrasound; Membrane pore resealing; Calcium; Voltage clamp

1. Introduction

Safe and efficient intracellular delivery of drugs and genes is critically important in targeted cancer treatment and gene therapy applications. Many studies have demonstrated that ultrasound (US) can deliver DNA, proteins, and other formulations of molecules of interest into viable cells [1–8]. It has been hypothesized that US energy, often amplified by micro-bubble activities (e.g. bubble oscillation and collapse) [9–16], generates transient, non-specific pores on the cell membrane, a process termed sonoporation [14,17–19]. The transient pores allow a limited time window for the otherwise non-permeable extra-cellular agents to enter the cell.

Because non-ionizing US exposure can be non-invasively controlled in application location and duration, sonoporation may provide an advantageous, safe delivery strategy for *in vivo*

applications. Compelling results obtained recently have stimulated great interest in the development of sonoporation applications with exciting possibilities[1–8]. However, progress in the field is hindered by a lack of mechanistic understanding of the sonoporation process and its outcome beyond demonstrations of initial feasibility [20]. Challenges in several key aspects remain to be addressed before sonoporation can be used successfully in humans as an efficient and safe strategy: 1) lack of means to rationally determine optimal sonoporation parameters, including physical and biochemical factors, to ensure high delivery efficiency and consistent outcome; 2) lack of mechanistic understanding of the causes for the downstream, cellular bio-effects and organ-level impacts of sonoporation; 3) lack of valid correlation and capability for translating in situ results to in vivo environment. Clearly, tackling these difficult yet important tasks requires in-depth investigation of the sonoporation process and identification of the major factors affecting it.

The observation of stably enhanced intracellular uptake of markers and the expression of intentionally delivered genes in viable cells via sonoporation indicate the transient nature and small scale of the membrane poration process. The US

---

generated pores on the plasma membrane must reseal to prevent the loss of intracellular contents to ensure cell survival, thereby limiting efficient inward transmembrane passage of desired extracellular agents within a time window before the completion of pore resealing. Furthermore, repair of the membrane disruption is necessary to avoid intracellular overload of ions that might be toxic to the cell or serve as the triggering sources for other irreversible and reversible cellular processes such as apoptosis [21] and calcium oscillation [22], making the rate of resealing one of the key factors determining the uptake efficiency and post-ultrasound cell fate.

It is therefore of significance to understand the process of sonoporation resealing, yet it is a task challenged by the lack of appropriate techniques to study the transient and sub-micron process. Consequently, sonoporation studies have been largely limited to static post-US assays. While important knowledge can be obtained through such analysis, post-US assays inevitably overlook the actual transient process of cell poration. Selection and attempted optimization of sonoporation parameters have mainly relied on empirical results of delivery outcome obtained after sonoporation. However, it is likely that the US parameters determined this way are only associated with specific experimental conditions due to the complexity of the US–cell interaction and its coupling with surrounding bubble activities. Given the statistical variance of such interactions in large number of cells, post-US assays are usually inadequate to deterministically correlate ultrasound parameters with sonoporation outcome and to uncover cellular mechanisms of sonoporation in individual cells.

To address these challenges and to understand the mechanism of sonoporation, we demonstrated previously for the first time the feasibility of studying sonoporation at the single cell level in real time using the voltage clamp techniques [18,23]. The transmembrane current of single cell under voltage clamp was measured to assess the change of cell porosity in sonoporation. Before US application, the transmembrane current is close to zero at a constant membrane holding potential (voltage clamped) in the absence of activation of endogenous ion channels, as the whole cell membrane is regarded as a resistor with constant resistance [24,25]. In sonoporation, US generates pores on the membrane (the pores effectively reduce the membrane resistance), which allows ions to flow through the pores and results in change in transmembrane current. The transmembrane current is determined by the pore size and ion concentration gradient across the cell membrane. Therefore the transmembrane current can be used as a sensitive means to monitor the dynamics of US induced pores in a single cell with high temporal resolution and sensitivity [18]. The novel application of such electrophysiological techniques enables a time-resolved measurement of sonoporation at single cell level, providing a sensitive and quantitative means to investigate the sonoporation process. Our previous results demonstrated that calcium in the extracellular solution affects sonoporation resealing [18]. The current study focused on quantitative investigation of the effects of extracellular Ca^{2+} on the resealing of US induced membrane disruption; results of the study might provide important molecular insight into reversible sonoporation to guide optimal delivery outcome.

2. Methods

2.1. Xenopus oocytes preparation

Commonly used as a model system for electrophysiological recordings, the *Xenopus* oocyte was chosen as a membrane model system [18,23,26,27] to study sonoporation dynamics. The same protocol described in our previous papers [18,23] was used for this study, and the procedures of harvesting and preparation of *Xenopus* oocytes follow an animal protocol approved by our Institutional Animal Care and Use Committee. Briefly, adult *Xenopus laevis* females (NASCO, Fort Atkinson, WI) were anaesthetized by immersion in a 0.3% tricaine (Sigma, St. Louis, MO) solution for 20 min. Oocytes were taken through a small incision (0.5–1 cm) made in the frog's lower abdomen, which was subsequently sutured back together. The frogs were allowed to recover in fresh water. Oocytes were digested in collagenase (1 mg/ml in ND96 solution containing 96 mM NaCl, 2 mM KCl, 1.8 mM $CaCl_2$, 1 mM $MgCl_2$, 5 mM HEPES, with pH 7.60), followed by a manual defolliculation if necessary. The oocytes were used immediately in experiments or stored in ND96 solution at 18 °C for one or two days before use. The oocytes were placed into the ND96-based test solution with the desired $[Ca^{2+}]$ and $[Mg^{2+}]$ several ($\sim$3 to 7) min before sonoporation experiment. Each oocyte was used for only one exposure of US in the sonoporation experiment. The cells were kept in culture for up to 24–36 h after sonoporation to determine the survival rate.

2.2. Experimental setup for real time measurement of sonoporation

A 35 mm polystyrene BD Falcon™ bacteriological Petri dish (Fisher Scientific, Pittsburgh, PA) was used to house a single *Xenopus* oocyte (diameter 0.8–1.1 mm) containing 4 ml ND96 or modified ND96 (altered $[Ca^{2+}]$ or $[Mg^{2+}]$) solution with or without 0.1% Definity™ (Bristol-Myers Squibb Medical Imaging, N. Billerica, MA). The Petri dish has been tested to show to have minimal effect (>95% transmission) on the transmission of US pulses through the bottom. Definity™ is an US imaging contrast agent consisting of stabilized bubbles with a diameter of 1.1–3.3 μm (mean 2.2 μm) and was used as cavitation nuclei to facilitate sonoporation. The solution with Definity™ was made by diluting the original stock solution of Definity™ ($\sim$1.2×10^{-10} particles/ml) by 1000 times in ND96 solution. This concentration is within the range of in vivo concentration at meaningful locations resulted from a typical imaging dosage (10^5–10^7 particles/ml). The actual bubble concentration in the experiments was measured by counting the bubbles in selected sample volumes under the microscope before and after exposures to US.

Tone-burst US pulses of the desired duration and pressure amplitude were generated using an unfocused circular planar piezoelectric US transducer (Piezo Technologies, Indianapolis, IN) with a diameter of 2.54 cm and a center frequency 1.075 MHz, driven by a function/waveform generator (Model 33250A, Agilent Technologies, Palo Alto, CA) and a 75-W power amplifier (Model 75A250, Amplifier Research, Souderton, PA).

The experimental setup has a vertical configuration similar to our prior setup [18], where the US transducer was immersed in water aiming upward, and the Petri dish hosting the cell was placed 2.5 cm above the US transducer surface. Only the bottom of the Petri dish was below the water level to avoid mixing the water and solution in the dish. The water served as acoustic coupling for US transmission through the bottom of the Petri dish to irradiate the cell. Standing wave was expected inside the dish due to the duration of tone burst (0.2 s) and the solution–air interface. The actual acoustic pressure inside the Petri dish was measured at the location of the oocyte using a 40-μm calibrated needle hydrophone (Model HPM04/1, Precision Acoustics, UK) and calibrated with an US power meter (Model UPM-DT-10, Ohmic Instrument Co, Easton, MD, USA).

The voltage clamp techniques [24] were used to measure the transmembrane current of the oocyte to monitor sonoporation in real time. Microelectrodes (tip diameter ∼ 1 μm) made from glass pipettes (Warner Instrument Corp., Hamden, CT) using an electrode puller (Sutter Instrument Co., Novato, CA) were filled with 3 M KCl and had resistances between 0.3–1.2 MΩ. Two microelectrodes connected to a voltage clamp amplifier (Dagan CA-1B, Dagan Corp., Minneapolis, MN) [25] were inserted into the oocyte membrane to measure the transmembrane current when the membrane potential of the oocyte was clamped at −50 mV during recordings. Trigger signals from the voltage clamp system were used to control the activation of US, thereby allowing synchronized and continuous recording of the transmembrane current of a single oocyte before, during, and after US application[18]. The transmembrane current under voltage clamp was recorded continuously at a sampling rate of 1.0 kHz starting before US exposure and for up to 15 min to capture changes in cell membrane porosity resulting from US exposure. Statistically, multiple bubbles can be present in the vicinity of the membrane in our experiments. Therefore multiple pores may be generated at different locations distributed on the cell membrane. Since the whole cell clamp configuration measures the ion movement through all pores on the whole membrane, the measurement should not be affected by, nor be used to distinguish the locations of the pores and/or the electrodes.

3. Results

Similar to our previous results [18], no change in the transmembrane current was detected without US application or when US was applied (duration 0.2 s, acoustic pressure 0.3 MPa) without Definity™ in the bath solution. The current stayed at a constant, equilibrium level close to 0 μA (−50 mV membrane holding potential), indicating the absence of endogenous channel activation by US application. On the other hand, when US was applied in the presence of Definity™ (0.1%), the amplitude of the inward transmembrane current increased rapidly after US application, as shown by the examples in Fig. 1, indicating the creation of non-specific pores on the cell membrane. Although no direct measurement was conducted in this study, sonoporation appeared to occur as the result of inertial cavitation, or the rapid collapse of bubbles driven by a US field, as >98% of the initially
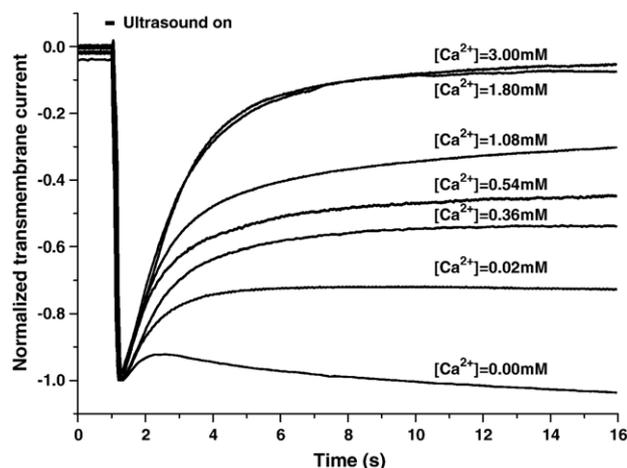

Fig. 1. Time-dependent inward transmembrane current recorded in oocytes under voltage clamp exposed to tone burst ultrasound (0.2 s duration, 0.3 MPa pressure amplitude) in the presence of 1% Definity® at different extracellular [Ca^{2+}]. The holding potential was −50 mV. Each current curve is normalized by the absolute value of its maximum which occurred at the end of ultrasound tone burst (1.2 s).

present Definity™ bubbles were destroyed after US application based on post-US bubble counting. It was also evident visually that the slightly milky solution became immediately clear after US exposure.

Fig. 1 includes examples of the inward (due to the −50 mV holding potential) transmembrane currents recorded in single cells during sonoporation in the presence of different [Ca^{2+}]. US tone burst of duration of 0.2 s was applied at 1 s after the start of the recording, indicated by the horizontal bar in the figure. Maximum change in the current occurred at the end of US pulse (at 1.2 s). For the convenience of comparison, each curve in the figure was normalized to the absolute value of the corresponding maximum current change (thereby the negative sign of the inward current is retained in the figure).

The maximal amplitude of the current change, usually on the order of 0.1–10 μA in our experiment, depends on the ionic concentration gradient across the cell membrane and the total area of the pores, which was determined by the US parameters used and the intrinsic properties of each individual cell in the experiment. For reversible sonoporation, where the cells survive, the transmembrane current exhibited an initial rapid increase reaching a maximal value, followed by a recovery process, and eventually returned to its pre-US level, indicating complete resealing of the pores.

3.1. Extracellular Ca^{2+} is required for resealing in sonoporation

Pore resealing or recovery of membrane disruption in sonoporation, as indicated by the transmembrane current returning to its pre-US level in our experiment, was found to require extracellular Ca^{2+} in our study.

As shown in the Fig. 1, the inward transmembrane currents recorded in single cells during sonoporation in solutions of different [Ca^{2+}] indicate that the resealing process in sonoporation was affected by the [Ca^{2+}]. In general, the transmembrane current

increased in amplitude followed US exposure and underwent a recovery process thereafter. At 1.8 or 3.0 mM [Ca²⁺], the transmembrane currents have similar dynamics and returned almost to their pre-US level by 15 s. In contrast, for cells in calcium-free solution (0 Ca²⁺ with 1 mM EGTA added as Ca²⁺ chelator), the transmembrane current exhibited minimal recovery with no sustained trend after sonoporation throughout the whole recording period in our experiment (data in later times up to 15 min not shown). However, when Ca²⁺ was added into the previously Ca²⁺-free solution (∼2 mM final concentration), recovery of current was initiated within a few seconds after the addition of calcium and reached pre-US level within 15–40 s thereafter (data not shown), similar to those cells originally in the 1.8 or 3 mM Ca²⁺ solution.

In general, lower [Ca²⁺] resulted in slower, weaker resealing, and often partial recovery of current was observed. A threshold of 0.54 mM was found for complete recovery. Fig. 2A shows the final percentage of transmembrane current recovery achieved (∼15 min in our experiments) at different [Ca²⁺]. No complete recovery was observed for cells when [Ca²⁺]< 0.54 mM; in such cases, the transmembrane current stayed at a level significantly below 100% (normalized by its maximum value), indicating failure of pore resealing. On the other hand, recovery of transmembrane current continued beyond 15 s when [Ca²⁺] >0.54 mM, and the cells were able to achieve complete recovery eventually. Furthermore, complete recovery was found to relate to cell survival (Fig. 2B). The cells that failed to achieve complete resealing died eventually after a period of time ranging from minutes to hours, determined by visible loss of intracellular contents and degeneration of cellular integrity, observed under the microscope (inset in Fig. 2B). Each of the images included in the inset in Fig. 2B shows a single oocyte with a diameter of about 1 mm, taken under a regular low magnification microscope (SM-4TY, American Scope Inc., Chino, CA). The oocytes are shown with pigmented dark brown in one hemisphere (animal hemisphere) and the bright hemisphere (vegetal hemisphere). The pores that failed to reseal in the absence of Ca²⁺ can often be seen in the images (inset in Fig. 2B).

Our previous study indicated that the resealing of the pores requires Ca influx into the cell [18]. The electrochemical gradient that is generated by the −50 mV holding potential and high extracellular [Ca²⁺] drives extracellular Ca²⁺ into the cell to mediate the resealing process. The entry of Ca²⁺ into the cell cannot be through calcium channels that are endogenous in the oocytes membrane because these channels are open only at membrane potentials more positive than −50 mV [24]. At the holding potential of −50 mV, no Ca²⁺ currents can be or were recorded through the membrane of oocytes.

3.2. Multiple dynamic processes and [Ca²⁺] dependent early-stage resealing

It is observed in our experiments that rapid recovering of transmembrane current occurred immediately after US exposure but became slower in a few second (Fig. 1), and that the recovery slowed down even further thereafter, suggesting the involve-
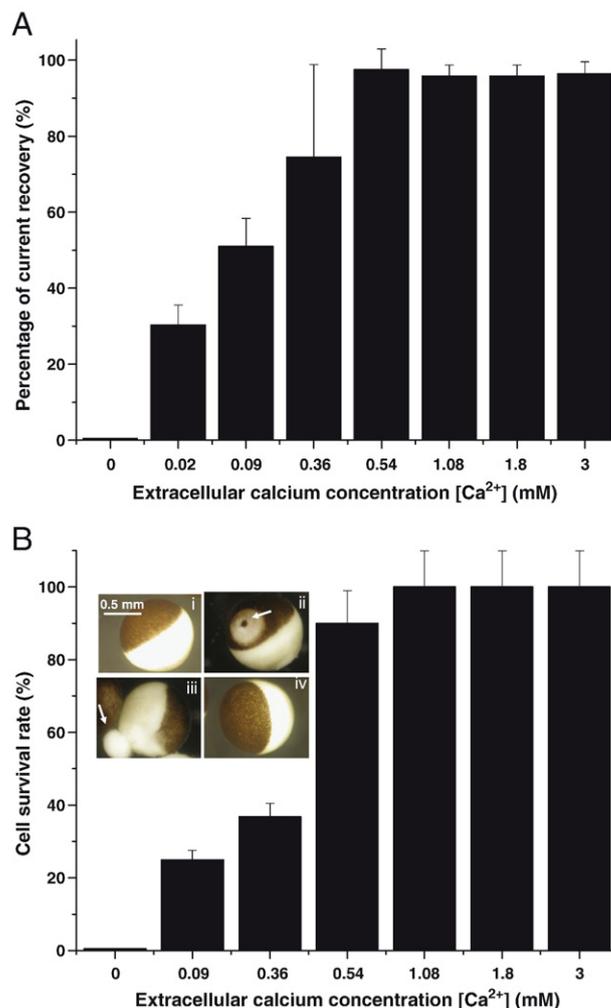

Fig. 2. Cell resealing and survival at different extracellular [Ca²⁺]. A) Percentage of the transmembrane current recovery from the maximum value in the presence of 0.02, 0.09, 0.36, 0.54, 1.08, 1.8, and 3.0 mM extracellular [Ca²⁺] with n=13, 10, 19, 10, 12, 20, and 11, respectively. B) Percentage of survived cells at extracellular [Ca²⁺] of 0, 0.09, 0.36, 0.54, 1.08, 1.80, and 3.0 mM with n=12, 8, 19, 19, 8, 21, and 11, respectively. Inset: Light micrograph images of *Xenopus* oocytes, showing a single oocyte before sonoporation (i), one oocyte with an un-sealed pore (arrow) where discoloration around the un-sealed pore is apparent (ii), a degenerating oocyte with leaking cytoplasmic contents (arrow) in the absence of Ca²⁺ (iii), and a recovered oocyte after sonoporation in the presence of 1.8 mM Ca²⁺ in solution (iv).

ment of different processes in the recovery of the transmembrane current. For the convenience of discussion, the resealing before 15 s is hereafter regarded as the early-stage recovery and the resealing afterwards, the late-stage recovery. The choice of 15 s was based on observation of the general time scales in the transmembrane current recordings of cell recovery in the presence of 1.8 or 3 mM Ca²⁺.

The involvement of multiple dynamic processes in resealing can be illustrated by the example in Fig. 3, where the normalized recovering transmembrane current after US was shown to be fitted successfully by a two exponential functions. Mathematically, the early-stage (<15 s) inward transmembrane current after US $I(t)(t>1.2$ s), can be expressed by a superposition of two exponential functions with rate constants k_f and k_s (noted as
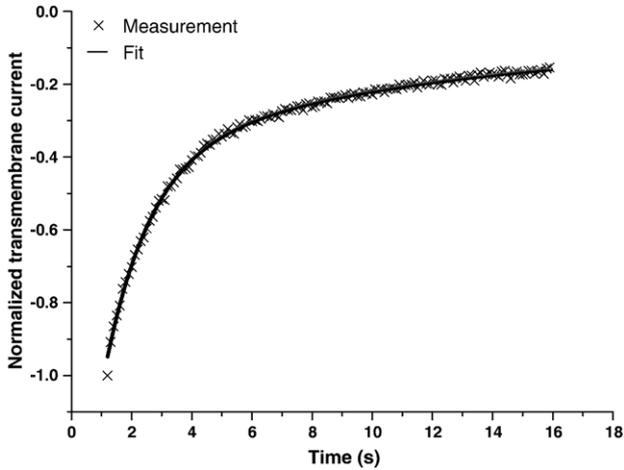
Fig. 3. Multiple dynamic processes in sonoporation resealing. An example of the normalized transmembrane current measured at $[Ca^{2+}]=1.8$ mM was shown to fit well by a superposition of two exponential functions with different rate constants 0.094 and 0.67 respectively.

fast and slow process) respectively, $I(t')=-I_{-15}-I_f \exp(-k_f t')-I_s \exp(-k_s t')$ with the associated amplitudes I_f and I_s for the fast and slow process. In the equation, $t'=t-1.2$ s is the time after US application (for convenience, t' is noted as t from here on), I_{-15} is the transmembrane current at 15 s after US application. A zero I_{-15} indicates complete recovery while a larger value correlates with weaker resealing. The maximal current change is therefore represented by $I_{max}=I_{-15}+I_f+I_s$. A normalized expression of the inward transmembrane current is obtained by dividing the current by I_{max} as $\hat{I}(t)=-\hat{I}_{-15}-\hat{I}_f \exp(-k_f t)-\hat{I}_s \exp(-k_s t)$.

In order to assess the early-stage recovery, $\hat{I}_{-15}$ as a function of $[Ca^{2+}]$ is shown in Fig. 4, where the decreasing $\hat{I}_{-15}$ values clearly show inhibited recovery at lower $[Ca^{2+}]$. No $\hat{I}_{-15}$ for 0 Ca^{2+} is included in the figure because the cells in calcium-free solution exhibited no recovery and the transmembrane current often became even larger and irreversible as the cells degenerated gradually, making $\hat{I}_{-15}$ meaningless in this case. It is interesting to notice that the presence of even very low $[Ca^{2+}]$ (e.g. 0.02 mM) promoted some resealing which delayed membrane degeneration and rupture (Fig. 4).

The best least square fitting parameters (k_f, k_s, $\hat{I}_f$, $\hat{I}_s$) for $\hat{I}(t)$ by the two exponential functions described above are shown in Fig. 5. No values at 0 Ca^{2+} are included because no recovery was observed for cells in Ca^{2+} free solution. Additionally, neither k_s or $\hat{I}_s$ values are included for $[Ca^{2+}]=0.02$ mM because the transmembrane current for cells at $[Ca^{2+}]=0.02$ mM can be fitted with one exponential function with rate constant k_f, thus inclusion of the process of k_s was not necessary. As shown in Fig. 5A and B, both rate constants k_f (0.79–1.19 s^{-1}) and k_s(0.11–0.21 s^{-1}) show no definite trend with varying $[Ca^{2+}]$; values of k_s are significantly lower than those of k_f. Thus process with rate constant k_s is regarded as slow resealing and the process with rate constant k_f the faster resealing process.

Fig. 5C shows that $\hat{I}_f$, the amplitude of the fast resealing process, increased with increasing $[Ca^{2+}]$, and was more than 3

times at 1.8 mM ($\sim 80\%$) than at 0.02 mM (20–25%), indicating that the calcium-dependent fast resealing process is dominant at higher $[Ca^{2+}]$. The amplitude of the slow resealing process ($\hat{I}_s$) is relatively constant but small ($\sim 20\%$) for all concentration values above 0.09 mM Ca^{2+} (Fig. 5D). The slow resealing process appeared to have a higher threshold of initiation (0.09 mM) than the fast process, which was already present at 0.02 mM (Fig. 5C). These thresholds were lower than the threshold for the complete resealing (0.54 mM) necessary for the cell to survive (Fig. 2).

3.3. Ca^{2+} dependent late-stage resealing

The continued recovery of the transmembrane current after 15 s is regarded as a late-stage recovery, with a much slower rate constant and is also Ca^{2+} dependent. To better delineate the late-stage processes, let $\hat{I}_L(t)$ represent the recovering or decaying current after 15 s, so $\hat{I}_L(15)=\hat{I}_{-15}$. $\hat{I}_L(t)$ can be expressed in two parts, $\hat{I}_L(t)=\hat{I}_L'(t)+\hat{I}_0$, where $\hat{I}_0$ represents the non-recovered current at the end and $\hat{I}_L'(t)$ the dynamic part of the late-stage resealing. The dependence of the whole recovery process on extracellular $[Ca^{2+}]$ can be seen by the results in Fig. 6A, which shows the time duration required for the transmembrane currents to reach various percentage of transmembrane current recovery for 0.54 and 1.8 mM $[Ca^{2+}]$. $\hat{I}_L'(t)$ is seen in the recovery at later (>15 s) time points (Fig. 6A). The time required for cells to complete up to 40% recovery showed no difference between 0.54 mM (2.68±0.46 s) and 1.8 mM (2.46± 0.41 s), consistent with the observation of fast recovery before 15 s (Fig. 5). The time required for cells to complete more than 50% recovery of current showed increasing difference between 0.54 mM and 1.8 mM, with a considerably lower late-stage recovery rate at 0.54 mM than that at 1.8 mM. The time required for the cells to recovery 90% recovery at 0.54 mM calcium concentration (98±50 s, $n=10$) was about 6 times as long as
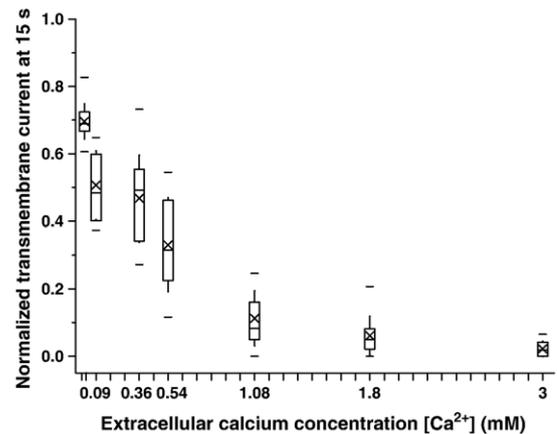

Fig. 4. Normalized transmembrane current (at 15 s) recorded in individual oocytes in the presence of different $[Ca^{2+}]$. The boxes at each concentration show 25th, 50th and 75th percentiles, respectively, cross symbols represent the mean value, the whiskers show the standard deviation, and the two dashes show the maximum and minimum values in the data in this and subsequent figures. The experiments with $[Ca^{2+}]=0$, 0.02, 0.09, 0.36, 0.54, 1.08, 1.8, and 3.0 mM had $n=12$, 14, 13, 19, 19, 12, 21, and 11, respectively.
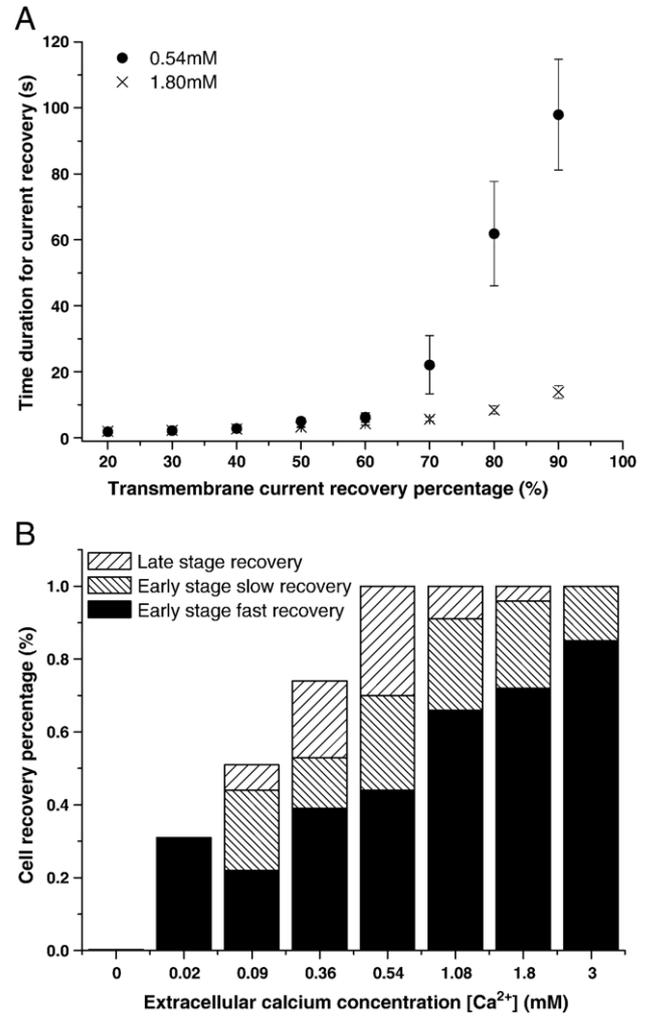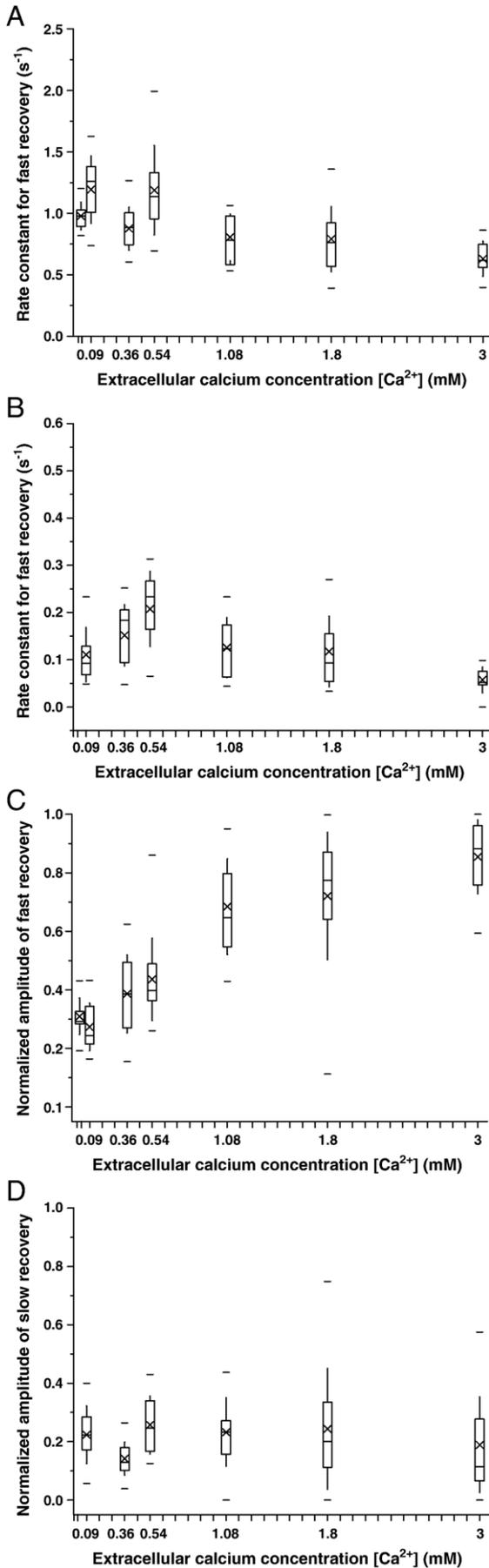
Fig. 6. Rate of transmembrane current recovery in sonoporation as a function of extracellular $[Ca^{2+}]$. A) Mean value of the time duration (and the standard error of the mean value) required for cell to reach current recovery at 0.54 mM and 1.8 mM Ca^{2+}. B) Stack column plot of the mean values for the early-stage fast ($\hat{I}_f$) and slow resealing processes ($\hat{I}_s$), and late-stage slow resealing process ($\hat{I}_L$). The respective sample sizes for $[Ca^{2+}]=0.02, 0.09, 0.36, 0.54, 1.08, 1.80$, and 3.0 mM are $n=14, 13, 19, 19, 12, 21$, and 11, respectively.

that at 1.8 mM (17.6 ± 12.8 s, $n=20$), although large variation existed among the cells.

Fig. 6B shows the components constitutes the maximum current, $\hat{I}_{max}=\hat{I}_0+\hat{I}'_L(\infty)+\hat{I}_s+\hat{I}_f$, including the early-stage fast ($\hat{I}_f$) and slow ($\hat{I}_s$) recovery, and the late-stage slow recovery ($\hat{I}'_L(\infty)$). The infinity symbol is used to indicate the end of the measurement. It can be seen from Fig. 6B that the Ca^{2+} threshold for fast recovery is 0.02 mM and that the early-stage

Fig. 5. Fitting parameters describing the early-stage dynamic recovery process of transmembrane current as a function of extracellular $[Ca^{2+}]$. A) Rate constant of fast recovery process vs. extracellular $[Ca^{2+}]$. B) Rate constant of slow recovery process vs. extracellular $[Ca^{2+}]$. C) Normalized amplitude of fast recovery process by the absolute value of maximum current change vs. extracellular $[Ca^{2+}]$. D) Normalized amplitude of slow recovery process by the absolute value of maximum current change vs. extracellular $[Ca^{2+}]$. The respective sample sizes for $[Ca^{2+}]=0.02, 0.09, 0.36, 0.54, 1.08, 1.80$, and 3.0 mM are $n=14, 13, 19, 19, 12, 21$, and 11.
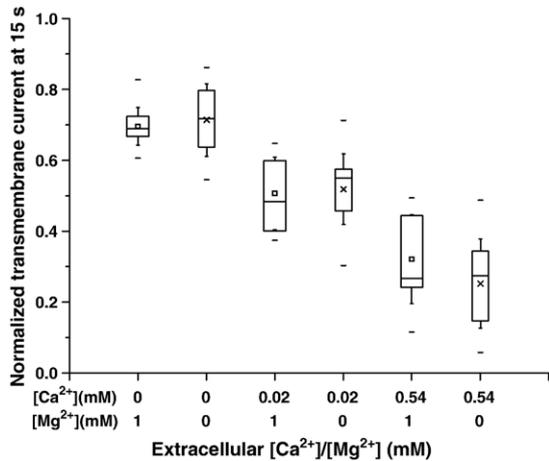
Fig. 7. Normalized transmembrane current at 15 s as a function of $[Mg^{2+}]$ and $[Ca^{2+}]$. The transmembrane currents are shown for cells in the presence 0 or 1 mM $[Mg^{2+}]$ and 0.02, 0.09, and 0.09 mM $[Ca^{2+}]$. The sampling sizes are $n = 14, 18, 13, 15, 10$ and 21 for the groups from left to right.

slow recovery and late-stage recovery had the same threshold at 0.09 mM. At sufficiently high $[Ca^{2+}]$ (e.g. 1.8 mM), robust early-stage fast and early-stage slow recovery achieve almost complete recovery, while the cells in lower $[Ca^{2+}]$ (e.g. 0.54 mM) achieved complete recovery after a much longer time duration.

3.4. Effects of extracellular Mg^{2+} on resealing process

To test whether 1 mM $[Mg^{2+}]$, present in ND 96 solution, has antagonizing effect on cell membrane resealing in sonoporation, a set of experiments were conducted to measure sonoporation in oocytes in modified ND96 solutions without Mg^{2+} (0 Mg^{2+}). Fig. 7 shows the comparison of $\hat{I}_{-15}$ for 0 $[Mg^{2+}]$ and 1 mM $[Mg^{2+}]$ and various $[Ca^{2+}]$ (0.02 mM, 0.09 mM, and 0.54 mM). No statistically significant difference was observed between 0 $[Mg^{2+}]$ and 1 mM $[Mg^{2+}]$ groups for the same $[Ca^{2+}]$, indicating no Mg^{2+} (1 mM) antagonism in early-stage cell membrane resealing at these $[Ca^{2+}]$. $\hat{I}_{-15}$ shows similar dependence on $[Ca^{2+}]$ as Fig. 4 with higher $\hat{I}_{-15}$ values at lower $[Ca^{2+}]$. The other fitting parameters (k_s, k_f, $\hat{I}_s$, $\hat{I}_f$) from the two exponential function fit also showed no statistically significant difference between the 0 $[Mg^{2+}]$ and 1 mM $[Mg^{2+}]$ group (data not shown). There is also no statistically significant difference for the late-stage resealing for these groups (data not shown). All these suggest the absence of Mg^{2+} antagonism on the resealing in sonoporation.

3.5. The effects of transmembrane current amplitude

The maximum transmembrane current change in sonoporation measured in our experiment exhibited a range of values (0.1–10 μA). The spread may have come from a number of sources including those associated with inherent cellular differences, variations from the micro-bubble concentration, size, and state, as well as the statistical nature of bubble activities in the vicinity of the cell membrane. For example, the mean

bubble concentrations in our experiment was $(9.0 \pm 3.2) \times 10^6$/ml ($n = 20$) ranging from 6.1×10^6/ml to 14.8×10^6/ml. Under the experimental conditions used in this study, it is likely that multiple pores were generated. As the transmembrane current has contributions from all pores, the variation in measured current amplitude suggests variation in pore size and number, in addition to the contribution from intrinsic cellular differences, which may have played an important role in addition to bubble concentration in the spread of measured currents. However, this current study cannot deterministically conclude which of these factors dominated in the measurement variation.

In order to test whether membrane resealing depended on the maximum transmembrane current resulted from sonoporation, the resealing characteristics are compared at different maximum transmembrane current. Fig. 8A is a scatter plot in semi-logarithmic scale in horizontal axis showing the actual amplitude of the transmembrane current (not normalized) at 15 s after US exposure, I_{-15}, vs. the maximum transmembrane current change (I_{max}) for 0.02 mM, 0.54 mM, and 1.8 mM $[Ca^{2+}]$. The data for
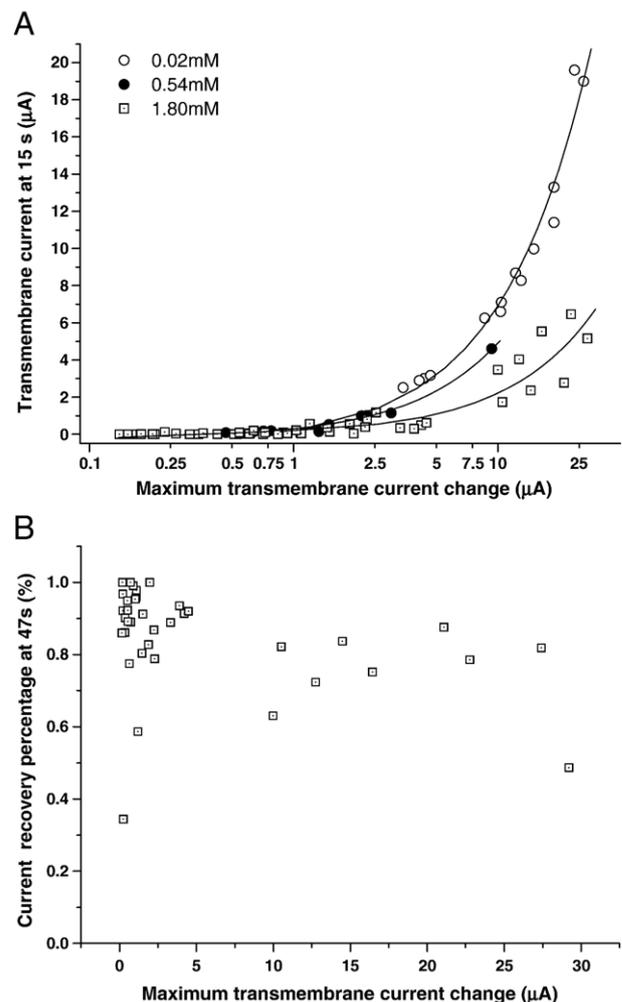

Fig. 8. Early- and late-stage recovery as a function of maximum transmembrane current. A) Scatter plots and linear regression fits show I_{15} vs. I_{max} plotted in logarithmic scale at 0.02 ($n = 14$), 0.54 ($n = 10$), and 1.8 mM $[Ca^{2+}]$ ($n = 47$). B) Scatter plot shows transmembrane recovery percentage in late-stage (47 s) vs. I_{max} at $[Ca^{2+}] = 1.8$ mM ($n = 37$).

each concentration was fitted by linear regression and plotted on a semi-logarithmic scale in I_{max}. The excellent agreement of the measurements and linear fitting curve demonstrates a linear relationship of I_{-15} with I_{max}, indicating that the early-stage recovery percentage (i.e., normalized $\hat{I}_{-15}$, Fig. 3) was not affected by I_{max}, consistent with our earlier findings [18]. The late-stage recovery percentage was slightly slower for larger I_{max}, as shown in Fig. 8B. When I_{max} was between 5 µA and 25 µA (0.75 ± 0.12, $n = 9$), the recovery percentage was slightly lower than that for cells with I_{max} below 5 µA (0.88 ± 14, $n = 28$) ($p < 0.007$).

4. Discussion

The results presented in this report demonstrate quantitatively for the first time that extracellular Ca^{2+} was required for reversible sonoporation and that the resealing of pores involved two or more distinctive processes, all affected by extracellular $[Ca^{2+}]$. This conclusion is made based on the following findings from the real time recordings of transmembrane current of single Xenopus oocytes under voltage clamp: 1) no recovery of transmembrane current was detected and incomplete recovery led to cell death in Ca^{2+} free solution; 2) complete recovery of transmembrane current and cell survival required extracellular $[Ca^{2+}] > 0.54$ mM and the recovery rate increased with increasing $[Ca^{2+}]$; 3) the recovery dynamics exhibited several different $[Ca^{2+}]$-dependent processes during the course of recovery. Descriptions of these important aspects of the sonoporation mechanism are novel and are made possible by the unique ability of voltage clamp techniques to monitor in real time the dynamic change in the membrane permeability in sonoporation at the single cell level. These findings are significant in providing molecular insight to understand sonoporation mechanism and outcome in order to ultimately bring the technology into human applications, particularly given the involvement of Ca^{2+} in triggering and controlling various important cellular processes.

Specifically, our results quantitatively characterize the involvement of different Ca^{2+}-dependent processes in sonoporation recovery. First, the rate constant for the fast recovery process did not appear to be affected by $[Ca^{2+}]$ (Fig. 5A) but its amplitude increased significantly with increasing $[Ca^{2+}]$ (Fig. 5C), suggesting a cellular process with enhanced recruitment by higher Ca^{2+} concentrations. This process is observed in very low extracellular $[Ca^{2+}]$ (0.02 mM) (Fig. 5A and C), and possibly even in 0 Ca^{2+} (Fig. 1), suggesting that the process may happen at the level of intracellular $[Ca^{2+}]$ (0–20 µM). On the other hand, the late-stage slow recovery of current exhibited an increased rate constant with increasing $[Ca^{2+}]$ (Fig. 6A) but the amplitudes of the late-stage slow process and early-stage slow process did not change with $[Ca^{2+}]$ (Figs. 5D and 6B), suggesting a cellular process regulated by high concentration of Ca^{2+} (>0.09 mM). Although the rate constant of the slow process k_s in the early-stage did not show a clear Ca^{2+} dependence, this could be due to the contamination of the fast process k_f in the fitting. The slow process may not be properly expressed in the presence of a dominant fast process. It is also possible that the early-stage slow process is a precursor of the late-stage slow process as they both have the threshold of

0.09 mM (Fig. 6B). It should be noted that while the choice of 15 s was somewhat arbitrary, it is a proper time scale representing the experimental observations that complete recovery occurs by that time at 1.8 mM Ca^{2+} and the rate constant for late-stage recovery process is more than an order of magnitude lower than the slow process before 15 s (Fig. 6A). The distinctive characteristics of the different processes have not been described in previous studies using less sensitive and static measurement techniques.

The absolute requirement of extracellular Ca^{2+} in sonoporation resealing and cell recovery is in contrast with the conventional notion regarding pore resealing in electroporation. Electroporation [28–31] is a technique that uses electric pulses to create pores in the cell membrane for delivery of desirable agents (e.g. genes or biologically active molecules) into cells. It is believed that pores created in electroporation are capable of self-resealing in the absence of calcium, driven by the tendency of the hydrophobic end of the lipid molecules to move from the energy unfavored membrane state with pores [29] to the lower energy resealed state.

On the other hand, work over the past two decades in the field of cell membrane disruption and repair has asserted that disruptions or pores in nucleated cell plasma membrane generally do not repair themselves spontaneously, but rather heal via an active, calcium-dependent process which most likely involves two functional components [32–35]: plasma membrane resealing by fusion of intracellular membrane compartments with each other and with the plasma membrane at the damage site, and cyctoskeletal reorganization. As the first step in cell repair, plasma membrane resealing has been shown to require extracellular calcium and has been temporally, spatially, and functionally related with rapid homotypic and heterotypic membrane fusion events associated with a calcium-regulated exocytosis process [34,36].

The resealing of plasma membranes is demonstrated necessary for cell survival in experiments where material is delivered to the cytoplasm by microinjection, chemical permeabilization, electroporation, and sonoporation. The process may be the same as that involved in the cell repair of the plasma membrane disruption occurring during normal physiological functions (e.g., cardiac contraction) and injury. The pores generated in electroporation reseal themselves in the absence of extracellular Ca^{2+} probably only because of the extremely small size of the disruptions observed, which usually are below 1 µm [37–39] and mostly in the range of 20–120 nm [40]. In such cases, resealing of the small holes, besides being driven by the energetically unfavorable situation, may also involve a process similar to the fast process observed in this study, which may bring complete resealing at very low extracellular $[Ca^{2+}]$ when the disruption is extremely small. Furthermore, it is possible that cells with larger disruptions did not survive in the absence of Ca^{2+} in electroporation, which is often accompanied by high cell death rate. Thus larger disruptions were not detected in post-electroporation assays.

The $[Ca^{2+}]$ threshold for cell membrane repair, below which repair fails to take place, has been recognized to vary by cell type and cell state. Recent work using sea urchin eggs and cultured cells has shown that plasma membrane repair requires

$[Ca^{2+}]$ above 0.3 mM [34,41]. Successful resealing required 10 to 30 s, but sometimes took as long as 90 to 120 s when the calcium concentrations were low, with a lower resealing rate at a lower level of $[Ca^{2+}]$ [42]. Membrane resealing durations in the range of 30–240 s for mammalian cells using fluorescent reporter molecules [33,34] have also been reported.

These results are in general agreement with our results for sonoporation resealing. However, no Mg^{2+} antagonism was observed in our study of sonoporation resealing for 1 mM Mg^{2+} in the solution, in contrast to the studies of cell wounding using laser and glass pipet tip in sea urchin eggs and cultured 3T3 cells, where much larger membrane disruptions were studied [32]. It is important to note that the measured threshold value of $[Ca^{2+}]$ for resealing depends on not only cell type and stage, but also possibly the means and extent of disruption, and it is also likely to be affected by the methods used to assess the resealing. Previous studies typically utilized fluorescence techniques such as monitoring of dye loss to gauge membrane resealing, which usually has less sensitivity, accuracy, and temporal resolution. Further studies are needed to investigate the reasons for these differences and the roles that the other factors described above may play in sonoporation resealing.

To complete the cellular repair, the cells must also restore the functionality of the damage site, which involving the cortical cytoskeleton in addition to membrane healing [35]. Study of wounding in amphibian eggs demonstrated that cytoskeleton repair response occurred 30–60 s after wounding and involves accumulation of F-actin and myosin-II around the wound site, which then coalesce into a circular array that contracts inward until the damage is covered. Importantly, the removal of extracellular calcium blocked healing and prevented recruitment of F-actin and myosin-II [43]. Studies in cultured fibroblast cells [44] showed similarly that membrane disruption stimulates cytoskeletal response that is Ca^{2+}-dependent, including disassembly of microtubules (MTs) around the wounding site, recruitment of end binding protein (EB1) to the MTs especially around the wound site, and subsequent elongation of MTs towards the wounding site. Such cytoskeletal response was found to require calcium at concentrations above 0.4 mM and has a higher rate at higher levels of $[Ca^{2+}]$. Furthermore, a time lapse of about 15–20 s is necessary for MT reassembly to occur after membrane disruption and can last for 60–140 s [45,46]. The range of the delays for these cytoskeletal responses to complete cell repair is comparable with the time scale of late-stage resealing of sonoporation observed in our experiment. It should be noted that it is unclear at this point whether the functional restoration of membrane can be precisely derived from the transmembrane current measurement, although such functional integrity does require normal ability of ion exchange through the membrane.

The fact that cells require Ca^{2+} to reseal suggests that a molecular mechanism is involved in regulating membrane resealing in sonoporation. The influx of Ca^{2+} might signal cell injury and trigger active mechanisms similar to those involved in cell repair of membrane injuries; such process rapidly seal membranes and ensure cell survival in sonoporation. The in-rush of Ca^{2+} may also play a role in signal transduction linked to downstream effects of sonoporation such as apoptosis [21] and calcium oscillation and calcium waves [22].

These results have important implications. There are a diverse range of diseases resulting from membrane repair defects, such as muscular dystrophy related cardiomyopathy [33]. Patients with such diseases resulted from cell membrane repair defects may not be appropriate candidates for sonoporation treatment as it may cause unwanted side effects. Furthermore, the remarkable effects of $[Ca^{2+}]$ on membrane resealing dynamics could be manipulated for practical use to achieve a (locally and transiently) controlled delivery outcome (e.g. slower resealing of pores may result in higher intracellular delivery efficiency).

The results presented in this paper establish a link between sonoporation and the almost omnipresent phenomenon of highly regulated cellular wound healing. The findings from studies of sonoporation resealing may shed new light on cellular wound healing, which is of considerable intrinsic interest. As a rapid emergency response, resealing is the process that cells need to repair membrane disruptions from physical or chemical insults and therapeutic interventions. It is also a normal cellular activity that commonly occurs as a natural consequence of tissue function. Failure to reseal leads to rapid cell death from loss of cytoplasm and consequential unabated Ca^{2+} influx, resulting in a direct loss of tissue integrity. Negative consequences can also ensue indirectly, from the release of proteases that attack neighbouring cells or even the provocation of an inflammatory response [35]. These aspects are relevant in assessing the safety of sonoporation applications.

5. Conclusion

Electrophysiology techniques, such as the voltage clamp method, provide a unique and sensitive means to investigate the sonoporation process at the single cell level. In this study, the time-resolved measurements of the transmembrane current of single *Xenopus* oocytes under voltage clamp were used to investigate the effects of extracellular Ca^{2+} on pore resealing in sonoporation. Our results demonstrated that Ca^{2+} plays an important role in regulating membrane resealing in sonoporation. Pore resealing exhibited multiple Ca^{2+} dependent processes with different characteristics and rate constants, including an early-stage fast recovery, followed by slower, late-stage recovery process. Complete resealing required extracellular $[Ca^{2+}]$ above a threshold and took longer at lower $[Ca^{2+}]$. These results reveal insights into the sonoporation mechanism and can be exploited for the design of safe and efficient sonoporation techniques by tuning the extracellular $[Ca^{2+}]$ to control the outcome in US gene/drug delivery applications.

References

[1] K. Zen, M. Okigaki, Y. Hosokawa, Y. Adachi, Y. Nozawa, M. Takamiya, T. Tatsumi, N. Urao, K. Tateishi, T. Takahashi, H. Matsubara, Myocardium-targeted delivery of endothelial progenitor cells by ultrasound-mediated microbubble destruction improves cardiac function via an angiogenic response, J. Mol. Cell. Cardiol. 40 (2006) 799–809.

[2] M. Shimamura, N. Sato, Y. Taniyama, S. Yamamoto, M. Endoh, H. Kurinami, M. Aoki, T. Ogihara, Y. Kaneda, R. Morishita, Development of efficient plasmid DNA transfer into adult rat central nervous system using microbubble-enhanced ultrasound, Gene Ther. 11 (2004) 1532–1539.

[3] T.P. McCreery, R.H. Sweitzer, E.C. Unger, S. Sullivan, DNA delivery to cells in vivo by ultrasound, Methods Mol. Biol. 245 (2004) 293–298.

[4] T. Nozaki, R. Ogawa, L.B. Feril Jr., G. Kagiya, H. Fuse, T. Kondo, Enhancement of ultrasound-mediated gene transfection by membrane modification, J. Gene Med. 5 (2003) 1046–1055.

[5] Q.L. Lu, H.D. Liang, T. Partridge, M.J. Blomley, Microbubble ultrasound improves the efficiency of gene transduction in skeletal muscle in vivo with reduced tissue damage, Gene Ther. 10 (2003) 396–405.

[6] S.L. Taylor, A.A. Rahim, N.L. Bush, J.C. Bamber, C.D. Porter, Targeted retroviral gene delivery using ultrasound, J. Gene Med. 9 (2007) 77–87.

[7] D.M. Hallow, A.D. Mahajan, M.R. Prausnitz, Ultrasonically targeted delivery into endothelial and smooth muscle cells in ex vivo arteries, J. Control. Release 118 (2007) 285–293.

[8] S. Chen, J.H. Ding, R. Bekeredjian, B.Z. Yang, R.V. Shohet, S.A. Johnston, H.E. Hohmeier, C.B. Newgard, P.A. Grayburn, Efficient gene delivery to pancreatic islets with ultrasonic microbubble destruction technology, Proc. Natl. Acad. Sci. U. S. A. 103 (2006) 8469–8474.

[9] R. Bekeredjian, C. Bohris, A. Hansen, H.A. Katus, H.F. Kuecherer, S.E. Hardt, Impact of microbubbles on shock wave-mediated DNA uptake in cells in vitro, Ultrasound Med. Biol. 33 (2007) 743–750.

[10] S. Mehier-Humbert, F. Yan, P. Frinking, M. Schneider, R.H. Guy, T. Bettinger, Ultrasound-mediated gene delivery: influence of contrast agent on transfection, Bioconjug. Chem. 18 (2007) 652–662.

[11] T. Kodama, Y. Tomita, K. Koshiyama, M.J. Blomley, Transfection effect of microbubbles on cells in superposed ultrasound waves and behavior of cavitation bubble, Ultrasound Med. Biol. 32 (2006) 905–914.

[12] H.R. Guzman, A.J. McNamara, D.X. Nguyen, M.R. Prausnitz, Bioeffects caused by changes in acoustic cavitation bubble density and cell concentration: a unified explanation based on cell-to-bubble ratio and blast radius, Ultrasound Med. Biol. 29 (2003) 1211–1222.

[13] A. van Wamel, K. Kooiman, M. Harteveld, M. Emmer, F.J. ten Cate, M. Versluis, N. de Jong, Vibrating microbubbles poking individual cells: drug transfer into cells via sonoporation, J. Control. Release 112 (2006) 149–155.

[14] P. Hauff, S. Seemann, R. Reszka, M. Schultze-Mosgau, M. Reinhardt, T. Buzasi, T. Plath, S. Rosewicz, M. Schirner, Evaluation of gas-filled microparticles and sonoporation as gene delivery system: feasibility study in rodent tumor models, Radiology 236 (2005) 572–578.

[15] M. Postema, A. van Wamel, F.J. ten Cate, N. de Jong, High-speed photography during ultrasound illustrates potential therapeutic applications of microbubbles, Med. Phys. 32 (2005) 3707–3711.

[16] P.P. Kamaev, J.D. Hutcheson, M.L. Wilson, M.R. Prausnitz, Quantification of optison bubble size and lifetime during sonication dominant role of secondary cavitation bubbles causing acoustic bioeffects, J. Acoust. Soc. Am. 115 (2004) 1818–1825.

[17] D.L. Miller, S.V. Pislaru, J.E. Greenleaf, Sonoporation: mechanical DNA delivery by ultrasonic cavitation, Somat. Cell Mol. Genet. 27 (2002) 115–134.

[18] C.X. Deng, F. Sieling, H. Pan, J. Cui, Ultrasound-induced cell membrane porosity, Ultrasound Med. Biol. 30 (2004) 519–526.

[19] S. Mehier-Humbert, T. Bettinger, F. Yan, R.H. Guy, Plasma membrane poration induced by ultrasound exposure: implication for drug delivery, J. Control. Release 104 (2005) 213–222.

[20] P. Campbell, M.R. Prausnitz, Future directions for therapeutic ultrasound, Ultrasound Med. Biol. 33 (2007) 657.

[21] L.B. Feril Jr., T. Kondo, Q.L. Zhao, R. Ogawa, K. Tachibana, N. Kudo, S. Fujimoto, S. Nakamura, Enhancement of ultrasound-induced apoptosis and cell lysis by echo-contrast agents, Ultrasound Med. Biol. 29 (2003) 331–337.

[22] R.E. Kumon, M. Aehle, D. Sabens, P. Parikh, D. Kourennyi, C.X. Deng, Ultrasound-induced Calcium Oscillations and Waves in Chinese Hamster Ovary Cells in the Presence of Microbubbles, Biophys. J. (2007).

[23] H. Pan, Y. Zhou, O. Izadnegahdar, J. Cui, C.X. Deng, Study of sonoporation dynamics affected by ultrasound duty cycle, Ultrasound Med. Biol. 31 (2005) 849–856.

[24] B. Hille, Ion Channels of Excitable Membranes, 3rd ed. Sinauer Associates, Inc., Sunderland, MA, 2001.

[25] W. Stuhmer, Electrophysiologic recordings from Xenopus oocytes, Methods Enzymol. 293 (1998) 280–300.

[26] J. Shi, G. Krishnamoorthy, Y. Yang, L. Hu, N. Chaturvedi, D. Harilal, J. Qin, J. Cui, Mechanism of magnesium activation of calcium-activated potassium channels, Nature 418 (2002) 876–880.

[27] Y. Masu, K. Nakayama, H. Tamaki, Y. Harada, M. Kuno, S. Nakanishi, cDNA cloning of bovine substance-K receptor through oocyte expression system, Nature 329 (1987) 836–838.

[28] H. Potter, Electroporation in biology: methods, applications, and instrumentation, Anal. Biochem. 174 (1988) 361–373.

[29] S.I. Sukharev, V.A. Klenchin, S.M. Serov, L.V. Chernomordik, A. Chizmadzhev Yu, Electroporation and electrophoretic DNA transfer into cells. The effect of DNA interaction with electropores, Biophys. J. 63 (1992) 1320–1327.

[30] J.C. Weaver, Electroporation theory. Concepts and mechanisms, Methods Mol. Biol. 55 (1995) 3–28.

[31] S.B. Dev, D.P. Rabussay, G. Widera, G.A. Hofmann, Medical applications of electroporation, IEEE, Trans. Plasma. Sci. 28 (2000) 206–223.

[32] R.A. Steinhardt, The mechanisms of cell membrane repair: a tutorial guide to key experiments, Ann. N. Y. Acad. Sci. 1066 (2005) 152–165.

[33] P.L. McNeil, R.A. Steinhardt, Plasma membrane disruption: repair, prevention, adaptation, Annu. Rev. Cell Dev. Biol. 19 (2003) 697–731.

[34] P.L. McNeil, T. Kirchhausen, An emergency response team for membrane repair, Nat. Rev. Mol. Cell Biol. 6 (2005) 499–505.

[35] W.M. Bement, H.Y. Yu, B.M. Burkel, E.M. Vaughan, A.G. Clark, Rehabilitation and the single cell, Curr. Opin. Cell Biol. 19 (2007) 95–100.

[36] P.L. McNeil, R.A. Steinhardt, Loss, restoration, and maintenance of plasma membrane integrity, J. Cell Biol. 137 (1997) 1–4.

[37] K.J. Muller, M. Horbaschek, K. Lucas, U. Zimmermann, V.L. Sukhorukov, Electrotransfection of anchorage-dependent mammalian cells, Exp. Cell Res. 288 (2003) 344–353.

[38] K.J. Muller, V.L. Sukhorukov, U. Zimmermann, Reversible electropermeabilization of mammalian cells by high-intensity, ultra-short pulses of submicrosecond duration, J. Membr. Biol. 184 (2001) 161–170.

[39] R. Shirakashi, C.M. Kostner, K.J. Muller, M. Kurschner, U. Zimmermann, V.L. Sukhorukov, Intracellular delivery of trehalose into mammalian cells by electropermeabilization, J. Membr. Biol. 189 (2002) 45–54.

[40] D.C. Chang, T.S. Reese, Changes in membrane structure induced by electroporation as revealed by rapid-freezing electron microscopy, Biophys. J. 58 (1990) 1–12.

[41] T. Togo, J.M. Alderton, G.Q. Bi, R.A. Steinhardt, The mechanism of facilitated cell membrane resealing, J. Cell Sci. 112 (Pt 5) (1999) 719–731.

[42] R.A. Steinhardt, G. Bi, J.M. Alderton, Cell membrane resealing by a vesicular mechanism similar to neurotransmitter release, Science 263 (1994) 390–393.

[43] W.M. Bement, C.A. Mandato, M.N. Kirsch, Wound-induced assembly and closure of an actomyosin purse string in Xenopus oocytes, Curr. Biol. 9 (1999) 579–587.

[44] T. Togo, Disruption of the plasma membrane stimulates rearrangement of microtubules and lipid traffic toward the wound site, J. Cell Sci. 119 (2006) 2780–2786.

[45] A.M. Sokac, C. Co, J. Taunton, W. Bement, Cdc42-dependent actin polymerization during compensatory endocytosis in Xenopus eggs, Nat. Cell Biol. 5 (2003) 727–732.

[46] A.M. Sokac, W.M. Bement, Kiss-and-coat and compartment mixing: coupling exocytosis to signal generation and local actin assembly, Mol. Biol. Cell 17 (2006) 1495–1502.